International Journal of Mechanical, Industrial and Aerospace Sciences
ISSN: 2517-9950
Vol:6, No:11, 2012

Stochastic Estimation of Cavity Flowfield

Yin Yin Pey, Leok Poh Chua, and Wei Long Siauw

***Abstract*—**Linear stochastic estimation and quadratic stochastic estimation techniques were applied to estimate the entire velocity flow-field of an open cavity with a length to depth ratio of 2. The estimations were done through the use of instantaneous velocity magnitude as estimators. These measurements were obtained by Particle Image Velocimetry. The predicted flow was compared against the original flow-field in terms of the Reynolds stresses and turbulent kinetic energy. Quadratic stochastic estimation proved to be more superior than linear stochastic estimation in resolving the shear layer flow. When the velocity fluctuations were scaled up in the quadratic estimate, both the time-averaged quantities and the instantaneous cavity flow can be predicted to a rather accurate extent.

***Keywords*—**Open cavity, Particle Image Velocimetry, Stochastic estimation, Turbulent kinetic energy.

I. Introduction

STOCHASTIC estimation was first presented by Adrian [1] as a means of estimating coherent structures in turbulent flows. It was later used by researchers to estimate an entire velocity field through utilizing instantaneous velocity at chosen positions [2]-[5]. This was possible as it was proven that the best mean square estimate of velocity fluctuation at position x+r is the conditional average of the velocity fluctuation at position at x+r given the velocity fluctuation at position x in the same instant, denoted by <u(x+r,t)|u(x,t)> [6]. In the recent years, researchers have started to use pressure events as the predictors in place of the instantaneous velocity [7]-[11]. Experimental techniques such as Particle Image Velocimetry (PIV) are limited in their ability to obtain time-resolved measurements. Hence, the ability to use pressure events to produce a low-dimensional, time-resolved description of flow through a small number of localized positions will contribute greatly to the ability of predicting and controlling the flow.

The current study employs instantaneous velocity magnitude at chosen reference positions as the estimators.

Using velocity magnitude to predict velocity flowfield has the advantage of utilizing only PIV images for the entire prediction process. This convenience brings about time and cost efficiency in the selection of estimator position since only 1 set of PIV results needs to be taken and the rest of the calculations are done in post-processing. Different combinations of predictor positions can be tested out before selecting the optimal combination for the best predicted flow. Thereafter, velocity sensors can be used at the selected estimator positions for the prediction of time-resolved flow within the cavity.

Y. Y. Pey and L. P. Chua are with the School of Mechanical and Aerospace Engineering, Nanyang Technological University, Singapore (e-mail: MLPCHUA@ntu.edu.sg).

W. L. Siauw is with DSO National Laboratories, Singapore.

As a preliminary study, random predictor positions were first selected to be tested. Linear Stochastic Estimation (LSE) was first carried out using 5, 9 and 13 estimators to check if the number of estimators and the estimator locations used in each case were sufficient in reconstructing the time-averaged features of the cavity flow. Thereafter, Quadratic Stochastic Estimation (QSE) was carried out on a chosen case to compare against the LSE results for additional flow features that could be resolved.

II. Background

The current study aims to estimate the entire velocity flowfield based on the velocity magnitude at selected reference positions. This is done by first estimating the velocity fluctuations in the streamwise and vertical direction (represented by u and v respectively) separately before adding the fluctuations to the mean velocity. The least mean square estimate for u can be written as

$$\tilde{u}_{ij}(\tau) = < u_{ij}(\tau) \mid E(\tau) > \tag{1}$$

where the subscripts i and j denotes the position in the 2-dimensional flow, E is the instantaneous velocity magnitude, U_{mag} and the angle brackets denote averaging. In the estimation process, U_{mag} has been normalized with the freestream velocity, U_∞ to give a similar order of magnitude for the estimator and the estimated variables. The conditional average can then be estimated by a power series [2]:

$$\tilde{u}_{ij}(\tau) = A_{ijn}E_n(\tau) + B_{ijop}E_o(\tau)E_p(\tau) + C_{ijqrs}E_q(\tau)E_r(\tau)E_s(\tau) + \ldots \tag{2}$$

where n refers to the number of estimators used.

The coefficients are obtained by minimizing the mean square error of the estimate, expressed as

$$e_{ij} = < [\tilde{u}_{ij} - u_{ij}]^2 > \tag{3}$$

where $\tilde{u}_{ij} = A_{ijn}E_n(\tau)$. By setting the derivation of the mean square error with respect to A to zero, the error can be minimized. This eventually reduces to

$$[A]=[E]^{-1}[V] \tag{4}$$

where [A] consists of a set of coefficients for every i, j and n chosen, [E] consists of the two-point correlation for U_{mag} and [V] is the correlation of U_{mag} with u.

Similarly, for quadratic estimate:

$$\tilde{u}_{ij}(\tau) = A'_{ijn}\, E_n(\tau) + B_{ijop} E_o(\tau) E_p(\tau) \quad (5)$$

A' is used in place of A to differentiate the linear coefficient in the quadratic estimate from the linear estimate. The difference in the two coefficients is accounted by the coupling of the linear and quadratic coefficients in the quadratic estimate. Again, by setting the derivation of the mean square error to zero, the error can be minimized. However, the derivative must now be found with respect to both A' and B. This reduces to

$$[C]=[E]^{-1}[V] \quad (6)$$

where [C] consists of the coefficients A' and B, [E] consists of the two-, three- and four-point correlations for U_{mag} and [V] is the two- and three-point correlations of U_{mag} with u.

The process of linear and quadratic estimation is done in a similar manner for v. More details of stochastic estimation can be found in [2], [7], [8], [12].

III. Experiment

A. Wind Tunnel

The wind tunnel used for this study is an open loop type as shown in Fig. 1. It has a test section size of 220cm (length) by 40cm (width) by 40cm (height) and turbulence intensity of less than 1% at 15m/s. The wind tunnel works by having a motor at the far end of the test section to induce air intake at the front. The air intake rate is varied by a control knob which changes the rotation speed of the impeller. Honeycomb is added in the inlet of the wind tunnel to smoothen the flow within the test section.

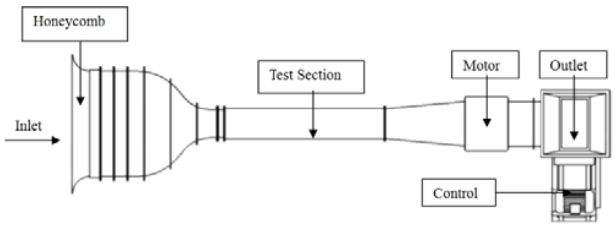

Fig. 1 Wind tunnel top view

B. Cavity configuration

The cavity tested has a length of L=80mm and depth of D=40mm, given a L/D ration of 2. x is taken to be the streamwise direction while y is taken to be the vertical direction. The width of the cavity spans the entire test section (i.e. 40cm) and the origin is taken to be at the leading edge of the cavity, along the centreline. A schematic diagram of the cavity along the centreline is shown in Fig. 2.

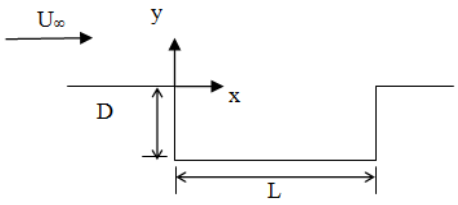

Fig. 2 Schematic of cavity centreline

A total of 3 different combinations of estimator locations were tested out. These combinations are shown in Fig. 3, as represented by the triangles. The exact locations of the estimators are recorded in TABLE . The first case has 5 equally spaced estimators at 2mm away from the cavity floor. The second case has the same 5 estimators as the first case, with 4 additional estimators: 2 at 2mm away from the leading wall and 2 at 2mm away from the trailing wall. The heights of these estimators are at $3/5$ and $4/5$ of the cavity height. The last case has the same 9 estimators as the second case, with 2 estimators added at $1/5$ of the cavity height and 2 estimators at $2/5$ of the cavity height. At each height, one estimator is 2mm away from the leading wall while the other is 2mm away from the trailing wall.

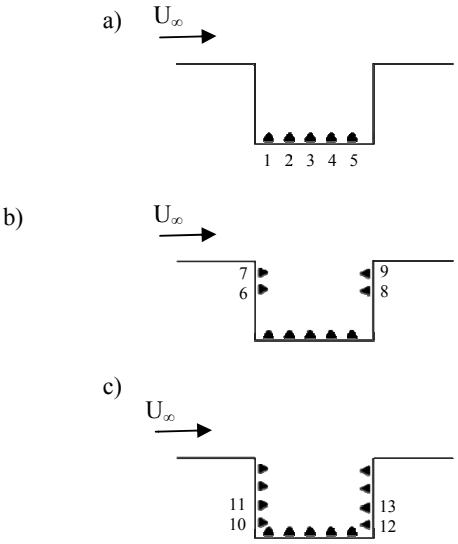

Fig. 3 Schematic of estimator positions in 3 test cases: a) case 1, b) case 2, c) case 3

TABLE I
ESTIMATOR LOCATIONS IN TEST CASES

Estimator	Case 1		Case 2		Case 3	
#	x(mm)	y(mm)	x(mm)	y(mm)	x(mm)	y(mm)
1	8	-38	8	-38	8	-38
2	24	-38	24	-38	24	-38
3	40	-38	40	-38	40	-38
4	56	-38	56	-38	56	-38
5	72	-38	72	-38	72	-38
6	-	-	2	-16	2	-16
7	-	-	2	-8	2	-8
8	-	-	78	-16	78	-16
9	-	-	78	-8	78	-8
10	-	-	-	-	2	-32
11	-	-	-	-	2	-24
12	-	-	-	-	78	-32
13	-	-	-	-	78	-24

C. Particle Image Velocimetry

The Particle Image Velocimetry (PIV) system used consists of a double pulsed Nd:YAG laser (EverGreen, Quantel), a HiSense MkII (Dantec Dynamics) camera and a system hub (FlowMap). The laser delivers 150mJ of energy per pulse at 532nm. The HiSense camera consists of a high resolution Hamamatsu C8484-05 digital CCD chip. This chip contains 1280 X 1024 light sensitive cells and an equal number of storage cells. The FlowMap System hub consists of a correlator unit, input buffer and a synchronization unit. The correlation unit determines the vector maps from the incoming image maps while the synchronization unit provides communication links between the processor and other elements in the PIV system such as the laser and camera.

The software FlowManager was installed on a computer to control the entire process of PIV measurement. When triggered by the user, a signal will be sent to the System Hub which will then fire the laser and acquire the images from the camera simultaneously. The System Hub hence synchronizes the laser with the camera. The time between a pair of laser pulses was set to be 200μs in FlowManager.

A schematic diagram of the PIV set up is shown in Fig. 4. The light sheet shines downwards through the test section ceiling to illuminate the centre plane of the cavity. A camera was positioned at the side of the test section to capture the flow in this plane.

The seeding particles used here was olive oil. These droplets are generated through a TSI Oil Drop Generator, where pressurized air atomizes oil in the generator reservoir. The droplets have a size of about 1μm.

A total of 700 pairs of time-independent images were obtained for the test case. For this total number of images, the values of Reynolds stresses at several positions along the cavity lip line (i.e. y=0) have been checked for statistical convergence. Each pair of images were adaptive correlated successively starting from an initial interrogation window size of 64 by 64 pixels to a final size of 16 by 16 pixels with a 50% overlap ratio. Subsequent post-processing of the PIV data was carried out in MATLAB.

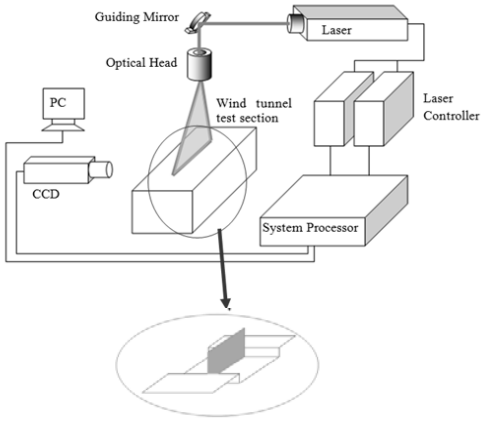

Fig. 4 Schematic of PIV set-up

D. Test Conditions

The experiments were carried out at a free stream velocity of 15m/s with Re_D=40000. The boundary layer was tripped by a 1mm thick tape 40cm upstream of the leading edge of the cavity. The turbulent boundary layer thickness was 14mm, and the momentum thickness was 1.5mm.

IV. RESULTS AND DISCUSSION

The estimated flowfield was reconstructed in each LSE test case and time-averaged quantities were calculated. These included the x-velocity (U) and y-velocity (V) contours, in-plane streamlines, normalized turbulent velocities in x and y directions (u'/U_∞ and v'/U_∞), Reynolds shear stress and turbulent kinetic energy, $0.5(u'^2+v'^2)$. The U and V contours, as well as the in-plane streamlines for the LSE cases resemble that of the original PIV data. This is due to the prediction process, which involves predicting the velocity fluctuations before adding back the mean flow. As such, these 3 plots are only presented for the original PIV data. Fig. 5 and Fig. 6 show the plots for the original PIV data and the 3 LSE test cases respectively. Note that the scale for the contour plots differs in each case.

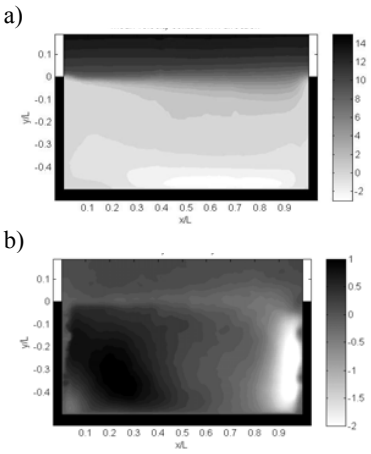

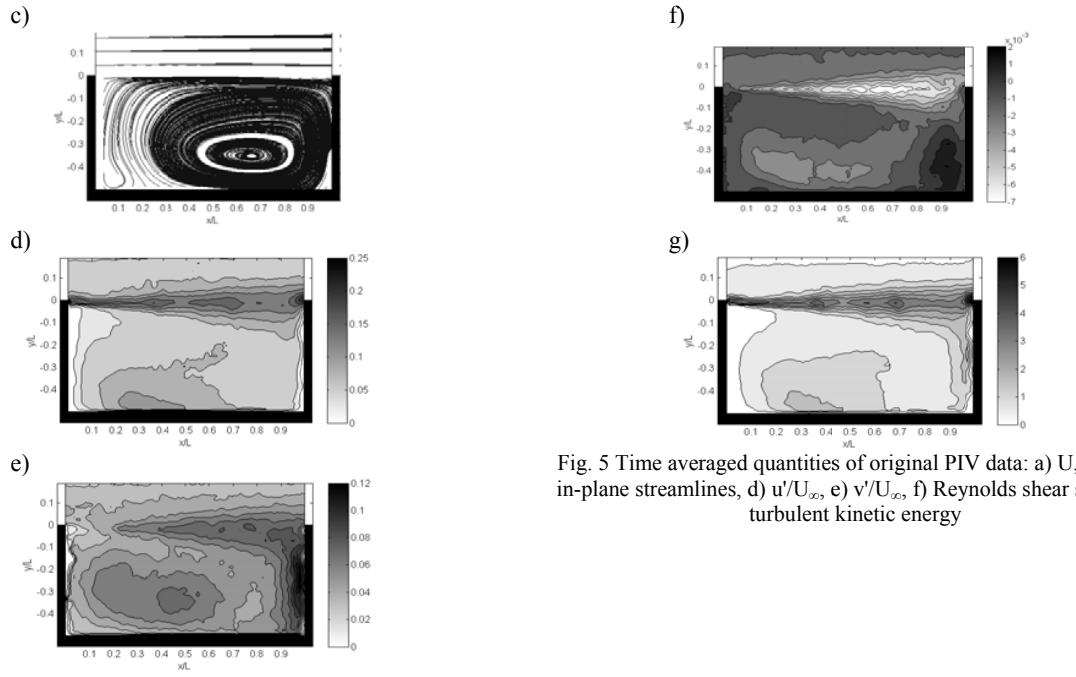

Fig. 5 Time averaged quantities of original PIV data: a) U, b) V, c) in-plane streamlines, d) u'/U_∞, e) v'/U_∞, f) Reynolds shear stress, g) turbulent kinetic energy

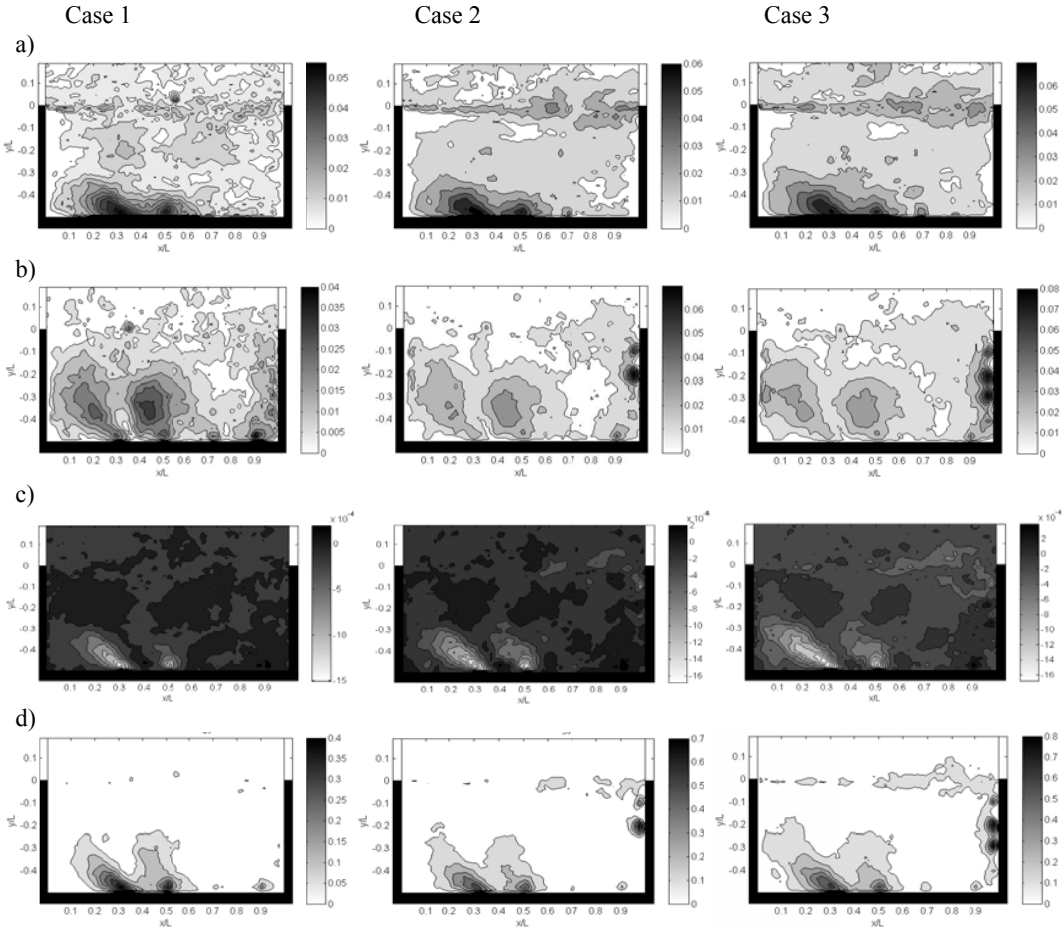

Fig. 6 Time averaged quantities of LSE test cases 1, 2 and 3: a) u'/U_∞, b) v'/U_∞, c) Reynolds shear stress, d) turbulent kinetic energy

From the LSE plots, it is observed that the kinetic energy level in the shear layer is being recovered increasingly as the number of estimator increases. The shear layer also appears to be more well resolved in case 3, as observed from the plot of u'/U_∞. In order to better evaluate the ability of the 13 chosen estimators in predicting the cavity flowfield, QSE was done on case 3. The time-averaged quantities from the estimated flowfield based on QSE are shown in Fig. 7. Note that in these plots, the velocity fluctuations have been scaled up by 5.5 times to match the magnitude of fluctuations in the original PIV data. This scale factor was obtained by comparing the turbulent kinetic energy, $0.5(u'^2+v'^2)$, of the QSE results to that of the original PIV data.

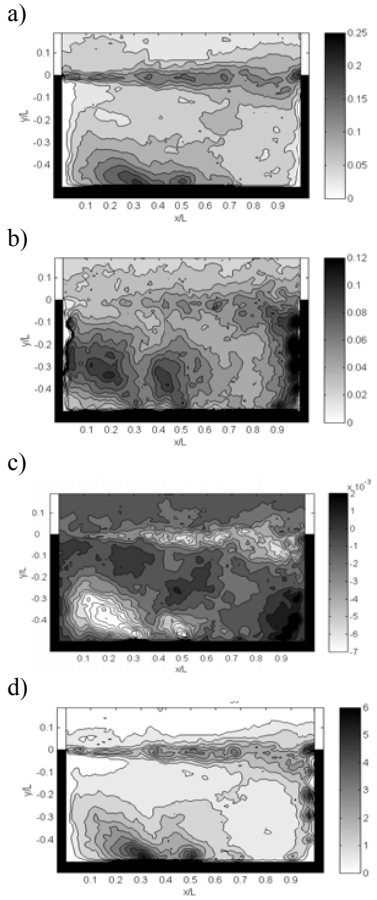

Fig. 7 Time averaged quantities of QSE test case, scaled up by 5.5 times: a) u'/U_∞, b) v'/U_∞, c) Reynolds shear stress, d) turbulent kinetic energy

Comparing Fig. 7 to Fig. 5, it seems that the distribution of u'/U_∞, v'/U_∞, Reynolds shear stress and turbulent kinetic energy can be predicted quite well. However there is a region of flow near the cavity floor, from x/L = 0.1 to 0.5 that appears to be over-predicted by the QSE method. In the plots of u'/U_∞, Reynolds shear stress and turbulent kinetic energy, a higher magnitude appears in the QSE case from y/L = -0.3 to the cavity floor, as compared to the original PIV data. As for the plot of v'/U_∞, a higher magnitude appears in the QSE case from y/L = -0.2 to the cavity floor, as compared to the original PIV data. Hence, the prediction is more accurate for flow within the shear layer, and less accurate towards the cavity floor. To further examine the accuracy of QSE in predicting the instantaneous flowfield, in-plane streamlines of 3 different snapshots were estimated and compared against the original PIV data. The comparisons are shown in Fig. 8.

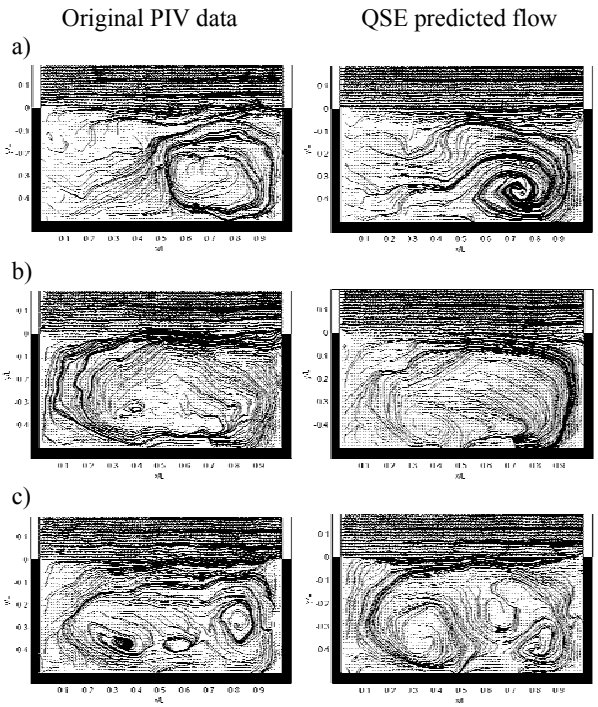

Fig. 8 Comparisons of instantaneous in-plane streamlines: a) snapshot 1, b) snapshot 2, c) snapshot 3

For each snapshot, the QSE is able to predict the general features of the instantaneous flows. For instance, snapshot 1 was relatively well predicted to have a recirculating region towards the trailing wall of the cavity while snapshot 2 was accurately predicted to have a large recirculating region that occupies the entire cavity. In order to further improve the prediction accuracy, more estimator positions are probably needed. Thus, depending on the extent of accuracy needed, a compromise should be sought between the computational time/resources needed and the prediction accuracy.

V. Conclusion

The current paper has explored the use of LSE and QSE in the prediction of cavity flow features. With LSE, the time-averaged quantities can be predicted better with increasing number of estimator positions. However, the shear layer of the original cavity flow is very poorly predicted by all LSE cases. When QSE was utilized, the predicted flow models the original flow very well, with a slight over prediction of flow quantities near the cavity floor. QSE also has the ability to predict the instantaneous flow, as proven by the comparisons of the instantaneous streamlines between the predicted flow and the original flow.

The study has shown the capability of using only 13 velocity magnitudes at carefully selected positions to predict

the flow field within an entire cavity. Hence, it should be possible to predict the time-resolved cavity flow if time-resolved velocity magnitudes are available. This could possibly facilitate and enhance active flow control since any change in the cavity flow may be detected through velocity changes at the selected position.

ACKNOWLEDGMENT

The support of DSO National Laboratories to this work is gratefully acknowledged.

REFERENCES

[1] R.J. Adrian, "On the Role of Conditional Averages in Turbulence Theory," in *Proceeding of the 4th Biennial Symposium on Turbulence in Liquids*. 1975: Univ. of Missouri, Rolla, MO.

[2] Y.G. Guezennec, "Stochastic estimation of coherent structures in turbulent boundary layers," *Physics of Fluids A (Fluid Dynamics)*, 1989. 1(6): pp. 1054-60.

[3] D.R. Cole, M.N. Glauser, and Y.G. Guezennec, "An application of the stochastic estimation to the jet mixing layer," *Physics of Fluids A (Fluid Dynamics)*, 1992. 4(1): pp. 192-4.

[4] D.R. Cole, and M.N. Glauser, "Applications of stochastic estimation in the axisymmetric sudden expansion," *Physics of Fluids*, 1998. 10(11): pp. 2941-9.

[5] S. Stokes, and M. Glauser, "Multi-point measurement techniques used in the study of separated flows," in *30th AIAA Fluid Dynamics Conference*, AIAA, Editor. 1999: Reno, NV.

[6] T.C. Tung, and R.J. Adrian, "Higher-order estimates of conditional eddies in isotropic turbulence," *Physics of Fluids*, 1980. 23(7): pp. 1469-70.

[7] A.M., Naguib, C.E. Wark, and O. Juckenhofel, "Stochastic estimation and flow sources associated with surface pressure events in a turbulent boundary layer," *Physics of Fluids*, 2001. 13(9): pp. 2611-26.

[8] N.E. Murray, and L.S. Ukeiley, "Estimating the shear layer velocity field above an open cavity from surface pressure measurements," in *32nd AIAA Fluid Dynamics Conference and Exhibit*, June 24 2002- June 26 2002. St. Louis, Missouri: AIAA.

[9] N.E. Murray, and L.S. Ukeiley, "Low-dimensional estimation of cavity flow dynamics," in *42nd AIAA Aerospace Sciences Meeting and Exhibit*, January 5, 2004 - January 8, 2004. Reno, NV, United states: American Institute of Aeronautics and Astronautics Inc.

[10] J.A. Taylor, and M.N. Glauser, "Towards practical flow sensing and control via POD and LSE based low-dimensional tools," *Transactions of the ASME. Journal of Fluids Engineering*, 2004. 126(3): pp. 337-45.

[11] L.M. Hudy, A. Naguib, and W.M. Humphreys, "Stochastic estimation of a separated-flow field using wall-pressure-array measurements," *Physics of Fluids*, 2007. 19(2): pp. 24103-1.

[12] R.J. Adrian, "Conditional eddies in isotropic turbulence," *Physics of Fluids*, 1979. 22(11): pp. 2065-70.